Temporal Instanton Analysis: Development and Implementation

Jonas A. Kersulis, *Student Member, IEEE, ...*

***Abstract*—A previously-developed method for studying a transmission network's vulnerability to wind forecast inaccuracy is expanded. The method uses optimization to find a likely wind generation pattern that brings a specified line to an unacceptably high temperature. The objective quantifies wind pattern likelihood in terms of distance from the forecast, respecting spatial and temporal correlation between wind sites and time intervals. The set of constraints enforces power balance and ensures a chosen line in the network reaches a fixed temperature by the final time step. The thermal constraint is second-order in voltage angle differences, and is based on a DC-approximate line loss formulation. Repeatedly solving the QCQP for all lines in the network yields a set of instanton candidate generation patterns, which may then be sorted by likelihood. Having described the temporal instanton QCQP and its solution, the paper turns to a discussion of implementation details. Finally, a series of numerical experiments is presented. These experiments demonstrate the effect of an instanton pattern on line temperature trajectory, the effects of wind covariance on instanton analysis, and algorithm scaling properties.**

***Index Terms*—forecast uncertainty, optimization, transmission operations, wind energy**

I. Introduction

A WIND forecast error that was once inconsequential is now vexatious. As wind grows into a major transmission-scale energy source, system operators find themselves frequently dealing with wind-induced network congestion [1]. Operators use wind forecast data to steer the network, but wind forecasts are significantly less accurate than generation and demand predictions [2]. Might forecast deviations compound across a collection of wind farms to overheat a transmission line? Which lines are most vulnerable to such an event? Temporal instanton analysis addresses these questions by identifying sag-inducing wind patterns and ranking them according to likelihood. The intersection of likely wind patterns with those that cause excessive line heating is of interest to system operators and planners, who may use this information to better prepare for renewable generation uncertainty.

Instanton analysis belongs to the family of distance to failure algorithms. It was introduced in [3] and [4], where the DC power flow approximation was used to represent a network's feasible operating region as a set of linear constraints. These constraints form the faces of a high-dimensional polytope that contains all feasible network states. Distance to failure is intuitively understood to be the shortest distance between an operating point and the surface of the constraint polytope. As shown in [4], one can use convex optimization to quickly find the smallest shift in wind generation that will drive the network to a chosen polytope face. Once every face has been considered, the collection of shifts may be sorted by distance from the forecast operating point. The wind pattern corresponding to the shortest distance between the forecast operating point and the boundary of the constraint polytope is termed the instanton; it is the smallest shift in wind generation that will drive the network to the brink of infeasibility.

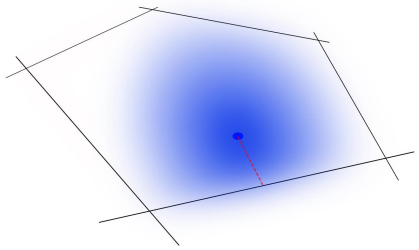

Fig. 1. How far is the forecast operating point from the edge of the feasible region, and might forecast inaccuracies drive the system there?

Instanton analysis research falls into two categories. The first is exploration of the trade-off between accuracy and complexity. Replacing the DC power flow approximation with the full AC model, for instance, yields greater accuracy at the cost of convexity [5]. Between the DC and AC extremes are various power flow approximations (see [6]–[8] for examples) which may be used to enhance accuracy while maintaining the solution guarantees of convexity. Regardless of the power flow model used, research in this category is ultimately focused on instantaneous vulnerability: find the smallest wind generation shift that drives a line to its steady-state power or current limit. This method uncovers previously hidden grid vulnerability, but may lead to overly-conservative decision making. It is safe to briefly operate a line above its current limit. As long as the line is allowed to cool before sagging to some limit (defined by statute and nearby trees), no harm is done. System operators know this; they periodically allow lines to operate above steady-state limits to promote smooth operation during congestion [9]. If an operator is comfortable with temporarily overloaded lines, information from instantaneous instanton analysis may be too conservative to aid decision making. Temporal instanton analysis, the second research category, seeks to overcome this limitation by modeling line temperature across multiple time steps.

In this paper we expound on the temporal instanton analysis method introduced in [10]. By modeling line temperature over

The authors are with the Department of Electrical Engineering and Computer Science, University of Michigan, Ann Arbor, MI 48104 USA (e-mail: kersulis@umich.edu; hiskens@umich.edu)

This work was supported by the Los Alamos National Laboratory Grid Science Program, subcontract 270958.

an appropriate time horizon, the proposed method discovers multiple-time-step wind patterns that are both likely to occur and sure to bring at least one line in the network to its temperature limit. The remainder of this paper is organized as follows. Section II describes the models at the core of temporal instanton analysis. Section III combines these models into a quadratically-constrained quadratic program (QCQP). The solution of this QCQP is described in Section IV. Section V contains results for two networks: a modified version of the RTS-96 and the larger WECC network. The former network has been used in previous instanton analysis studies, while the latter serves to demonstrate scalability of temporal instanton analysis. Finally, an appendix contains a detailed description of the thermal model used to calculate line temperature.

We expand on prior work by providing a more detailed treatment of the objective function, discussing implementation details including computational complexity and sparsity, and using an improved secular equation solution.

II. Models

Temporal instanton analysis entwines three physical phenomena. Transmission line temperature is based on a heat balance model, forecast error likelihood is quantified via a statistical model, and the feasible region of network operation is delineated using a network model. This section describes the three models in detail.

A. Transmission Line Heating

A simplified relationship between power flow and line temperature is key to making temporal instanton analysis tractable. Starting with an IEEE standard [11], we derive an approximate recursive relationship between a line's temperature at one time step and voltage angle differences at all previous time steps. This relation is summarized below. (Appendix A contains a detailed derivation.)

Consider a time horizon with n_t intervals, each on the order of ten minutes long. Power flow data is updated once per interval (at $t_1, t_2, \ldots, t_{n_t}$), but all other parameters (resistance, solar heating, etc.) remain constant. Choose a single transmission line in the network —suppose it lies between nodes i and j— and let this line's thermal limit be represented by $T_{\text{lim,C}}$ (°C). We can constrain the line's temperature at time t_{n_t} to be equal to this limiting value by enforcing the constraint

$$\sum_{k=1}^{n_t} \hat{\theta}_{ij}(t_k)^2 = \frac{a}{c}\left(T_{\text{lim,C}} - f\right), \tag{1}$$

where

$$\hat{\theta}_{ij}(t_k) = \theta_{ij}(t_k)\sqrt{(e^{a\bar{t}})^{n-k+1} - (e^{a\bar{t}})^{n-k}} \tag{2a}$$

$$a = \frac{1}{mC_p}\left[-\eta_c - 4\eta_r T_{\text{m,K}}^3\right] \tag{2b}$$

$$c = \frac{r_{ij} S_b}{3mC_p x_{ij}^2 L_{ij}} \tag{2c}$$

$$d = \frac{\eta_c T_{\text{a,C}} + \eta_r\left(4T_{\text{m,C}}T_{\text{m,K}}^3 + T_{\text{a,K}}^4 - T_{\text{m,K}}^4\right) + q_s}{mC_p} \tag{2d}$$

$$f = (e^{a\bar{t}})^n T_{\text{l,C}}^0 + \frac{d}{a}\left[\sum_{i=1}^{n}\left((e^{a\bar{t}})^i - (e^{a\bar{t}})^{i-1}\right)\right] \tag{2e}$$

In (2a), $\theta_{ij}(t_k)$ is the angle difference across line $i-j$ at time interval t_k, and $\bar{t}$ is the length of each time interval (e.g. $\bar{t} = t_k - t_{k-1}$). In (2b), a is a constant with units of s^{-1}; mC_p is the heat capacity in J/m-°C; η_c is the conductive heat loss rate coefficient in W/m-°C; η_r is the conductive heat loss rate coefficient in W/m-°C^4; and $T_{\text{m,K}}$ is the average of ambient temperature $T_{\text{a,K}}$ and limit temperature $T_{\text{lim,K}}$, in Kelvin. In (2c), c is a constant with units of W/m; r_{ij} and x_{ij} are the resistance and reactance of line $i-j$ in per unit, respectively; S_b is the system base (e.g. 100 MVA); and L_{ij} is the length of one phase of line $i-j$ conductor, in meters. In (2d), d is a constant with units of W/m, and q_s is the solar heat gain rate in W/m. Finally, in (2e), f is a constant with units of degrees Celsius, and $T_{\text{l,C}}^0 = T_{\text{l,C}}(t_0)$ is the line's initial temperature (based on generator dispatch and forecast) in Celsius.

B. Wind Forecast Inaccuracy

Distance from the forecast tends to approximate a particular deviation pattern's likelihood,[1] but spatial and temporal correlation add complexity. Consider several wind farms scattered across a transmission grid, each with a forecast power output. Let the error in this forecast be represented by a zero-mean Gaussian random variable.[2] Then the wind forecast deviation pattern for a single time step takes takes the form of a Gaussian random vector. Elements of this vector are correlated due to spatial relationships between wind sites: if wind speed increases at one site, for instance, a simultaneous decrease at a neighboring site is unlikely. In addition to spatial correlation, there may also be temporal relationships between wind farms.

Suppose a network has n_r wind sites and we wish to consider n_t time intervals. Let $\mathbf{r}$ be the $(n_t \cdot n_r) \times 1$ vector of forecast deviations across all wind sites and time intervals. The first n_t elements of $\mathbf{r}$ contain forecast errors for the first site at times t_1 to t_{n_t}, the second n_t are errors for the second site, and so on. The density function for $\mathbf{r}$ is

$$f(\mathbf{r}) = \frac{\exp\left(-\frac{1}{2}\mathbf{r}^\top \mathbf{C}^{-1}\mathbf{r}\right)}{(2\pi)^{\frac{n}{2}}\sqrt{\det \mathbf{C}}}\ , \tag{3}$$

where $\mathbf{C}$ is the correlation matrix. Maximizing f corresponds to minimizing $\mathbf{r}^\top \mathbf{C}^{-1}\mathbf{r}$. Thus, one may express a desire to maximize wind pattern likelihood with

$$\min\ \mathbf{r}^\top \mathbf{Q}\mathbf{r}, \tag{4}$$

where $\mathbf{Q} = \mathbf{C}^{-1}$ is the precision matrix. There are many ways to determine $\mathbf{C}$ or $\mathbf{Q}$ from historical data. The authors of [14] use maximum likelihood optimization to fit a set of parameters to observed data, thereby generating a sparse precision matrix. In our RTS-96 numerical study we assigned reasonable geographic coordinates to each wind site, then mapped distances between site pairs to correlation values using

[1] For independent power injections like conventional generators or demand nodes, this intuitive model may be adequate.

[2] For time scales shorter than roughly one hour, a Cauchy distribution is more appropriate, but forecast errors are commonly assumed to be Gaussian nonetheless. See [13].

Figure 2.10 of [15]. A third option is to compute a sample correlation matrix from time series data.

C. Network Model

Undesirable scenarios found by temporal instanton analysis are of no consequence if they are infeasible. We must therefore restrict our search to the feasible region using power flow constraints. We use a set of linear constraints corresponding to DC power flow with distributed slack.[3] The mismatch between total power generation and demand at any time step is divided over multiple generators according to participation factors. The next section expresses our power flow model mathematically.

III. Temporal Instanton QCQP

The following quadratically constrained quadratic program is a concise expression of our desire to find feasible, likely wind patterns that will cause one transmission line in the network to reach its temperature limit by the end of a certain time horizon:

$$\min_{\mathbf{r}} \quad \mathbf{r}^\top \mathbf{Q} \mathbf{r} \tag{5a}$$

subject to:

$$\sum_{k=1}^{n_t} \hat{\theta}_{ij}(t_k)^2 = \frac{a}{c}\left(T_{\text{lim,C}} - f\right) \text{ for some } (i,j) \in \mathcal{G} \tag{5b}$$

$$\sum_{j} Y_{ij}\theta_{ij,t_k} = G_{i,t_k} + (R_{i,t_k} + \mathbf{r}_{i,t_k}) - D_{i,t_k} \quad \forall i \in 1...n_b,\ k \in 1...n_t \tag{5c}$$

$$\mathbf{G}_{t_k} = \mathbf{G}_{0,t_k} + \alpha_{t_k}\mathbf{g} \quad \forall k \in 1 \dots n_t \tag{5d}$$

$$\theta_{ref,t_k} = 0 \quad \forall k \in 1 \dots n_t \tag{5e}$$

In (5), n_b represents the number of buses (nodes) in the network, n_t the number of time steps, and $\mathcal{G}$ the set of edges (transmission lines). The objective (5a) matches (4) and expresses a desire to find wind patterns that are likely to occur (see Section II-B). In this objective, $\mathbf{r}$ is the vector of wind output forecast errors, and $\mathbf{Q}$ is the precision (or inverse covariance) matrix. The first constraint (5b) forces the temperature of a particular line to reach $T_{\text{lim,C}}$ degrees Celsius at the final time t_{n_t}. (See Section II-A for a detailed explanation.) In (5c), which enforces DC power balance, Y_{ij} is the $[i,j]$-th element of the admittance matrix (which assumes zero resistance); θ_{ij,t_k} is the difference between voltage angles θ_i and θ_j at time t_k; G_{i,t_k} is conventional active power generation at node i and time t_k; $(R_{i,t_k} + \mathbf{r}_{i,t_k})$ is the sum of renewable generation forecast and forecast error for wind node i at time t_k (equal to zero if node i has no wind farm); and D_{i,t_k} is the power demand for bus i at time t_k. Constraint (5d) implements droop response: scheduled generation at time t_k is represented by the vector G_{0,t_k}, and each generator G_i compensates for of power mismatch α_{t_k} according to its participation factor $\mathbf{g}_i$. Finally, the constraint (5e) establishes the angle reference bus.

[3]DC power flow assumes a flat voltage profile, negligible line resistance (though resistance values are used to calculate line temperatures), and linearity of the sine function.

The mathematical program (5) has a quadratic objective function, a set of linear constraints, and a single quadratic constraint. We can emphasize this QCQP form by combining all variables into a single vector $\mathbf{z}$ and re-writing (5) as

$$\min \quad \mathbf{z}_1^\top \mathbf{Q}_{\text{obj}} \mathbf{z}_1 \tag{6a}$$

$$s.t. \quad \mathbf{z}_3^\top \mathbf{z}_3 = c \tag{6b}$$

$$\mathbf{A}\mathbf{z} = \mathbf{b}. \tag{6c}$$

The objective (6a) is equivalent to (5a), the quadratic equality constraint (6b) is equivalent to (5b), and the linear equality constraint (6c) combines (5c)-(5e). The vector $\mathbf{z}$ consists of $n_t \cdot (n_b + n_r + 2)$ variables, where n_t is the number of time steps, n_b the number of nodes, and n_r the number of nodes with wind generation. The matrix $\mathbf{A}$ has $n_t \cdot (n_b + 2)$ rows: there are $n_b \cdot n_t$ power flow equations (5c), n_t equations defining mismatch α at each time step, and n_t auxiliary angle variables defined according to (2a). Subscripts are used to distinguish variable types: $\mathbf{z}_1$ contains the $n_t n_r$ wind deviations $\mathbf{r}$, $\mathbf{z}_2$ contains the $n_t \cdot (n_b + 1)$ angle and mismatch variables, and $\mathbf{z}_3$ contains the n_t auxiliary angle difference variables involved in line temperature calculation (thereby causing (6b) to take the form of a norm constraint).

Solving (6) for each line in the network yields a set of instanton candidate wind patterns, each of which will heat a particular line to its thermal limit. Of these candidates, the one with lowest objective value is the instanton wind pattern. The next section contains a solution method for QCQPs of the form (6), based in part on work in [16].

IV. QCQP Solution Method

By now the difference between instantaneous and temporal analyses is clear. Instead of a quadratic program, whose solution readily obtained from KKT conditions, we have a QCQP. The root of this difference is the fact that one cannot express resistive losses—even approximately—as a linear constraint. QCQPs are NP-hard in general; solutions may exist, but unless the quadratic constraint matrices are positive-definite there is no solution guarantee [17]. Fortunately, our QCQP belongs to the family of trust region subproblems. As shown in [16], it may be solved in polynomial time. Our solution method, originally presented in [10], divides into four steps.

A. Translation

The first step is to change variables from $\mathbf{z}$ to $\mathbf{y} = \mathbf{z} - \mathbf{z}^*$, where $\mathbf{z}^* = \arg\min\{\|\mathbf{z}\| : \mathbf{A}\mathbf{z} = \mathbf{b}\}$. This translation transforms $\mathbf{A}\mathbf{z} = \mathbf{b}$ into $\mathbf{A}\mathbf{y} = \mathbf{0}$ without qualitatively altering the objective. To prevent the change from introducing a linear term into the quadratic constraint, we require $\mathbf{z}_3^* = \mathbf{0}$. Thus, we seek the min-norm solution to

$$\mathbf{A}\begin{bmatrix}\mathbf{z}_1^* \\ \mathbf{z}_2^* \\ \mathbf{0}\end{bmatrix} = \mathbf{b}. \tag{7}$$

It is straightforward to find $\mathbf{z}^*$ by taking the pseudoinverse of $\mathbf{A}$. After translation, the problem becomes

$$\min \quad \mathbf{y}_1^\top \mathbf{Q}_{\text{obj}} \mathbf{y}_1 + 2\mathbf{y}_1^\top \mathbf{Q}_{\text{obj}} \mathbf{z}_1^* \tag{8a}$$

$$s.t. \quad \mathbf{y}_3^\top \mathbf{y}_3 = c \tag{8b}$$
$$\mathbf{A}\mathbf{y} = \mathbf{0}. \tag{8c}$$

B. Kernel mapping

The form of (8c) suggests an intuitive explanation: any solution to (8) must lie in the nullspace (kernel) of $\mathbf{A}$. So long as there are no rows of zeros in the matrix of injection shift factors, $\mathbf{A}$ will have full row rank and a $n_t n_r$-dimensional nullspace. We can let $\mathbf{y} = \mathbf{N}\mathbf{x}$ where the $n_t n_r$ columns of $\mathbf{N}$ span $\mathcal{N}(\mathbf{A})$. This change of variables is akin to a rotation, but reduces the problem dimension to $n_t n_r$. After partitioning $\mathbf{N}$ so that

$$\begin{bmatrix}\mathbf{y}_1\\ \mathbf{y}_2\\ \mathbf{y}_3\end{bmatrix} = \begin{bmatrix}\mathbf{N}_1\\ \mathbf{N}_2\\ \mathbf{N}_3\end{bmatrix}\mathbf{x},$$

we can rewrite (8) in terms of $\mathbf{x}$:

$$\min \quad \mathbf{x}^\top(\mathbf{N}_1^\top \mathbf{Q}_{\text{obj}}\mathbf{N}_1)\mathbf{x} + 2\mathbf{x}^\top(\mathbf{N}_1^\top \mathbf{Q}_{\text{obj}}\mathbf{z}_1^*) \tag{9a}$$
$$s.t. \quad \mathbf{x}^\top \mathbf{N}_3^\top \mathbf{N}_3 \mathbf{x} = c. \tag{9b}$$

All feasible solutions to (9) lie in the nullspace of $\mathbf{A}$, so the linear constraints are now implicit.

C. Obtaining a norm constraint

After kernel mapping, the quadratic constraint is no longer a norm constraint. This can be corrected by a change of variables. Let $\mathbf{N}_3^\top = \mathbf{U}\mathbf{S}\mathbf{V}^\top$ and $\hat{\mathbf{x}} = \mathbf{U}^\top\mathbf{x}$. The constraint (9b) becomes

$$\mathbf{x}^\top \mathbf{U}\mathbf{S}\mathbf{S}^\top \mathbf{U}^\top \mathbf{x} = \hat{\mathbf{x}}^\top \mathbf{S}\mathbf{S}^\top \hat{\mathbf{x}} = c, \tag{10}$$

where $\mathbf{S}$ is diagonal with at most n_t nonzero elements. The right side of (10) may be expanded into

$$\begin{bmatrix}\hat{\mathbf{x}}_1^\top & \hat{\mathbf{x}}_2^\top\end{bmatrix}\begin{bmatrix}\hat{\mathbf{S}}^2 & \mathbf{0}\\ \mathbf{0} & \mathbf{0}\end{bmatrix}\begin{bmatrix}\hat{\mathbf{x}}_1\\ \hat{\mathbf{x}}_2\end{bmatrix}. \tag{11}$$

The second step is a change of variables from $\hat{\mathbf{x}}$ to $\mathbf{w}$ where

$$\begin{bmatrix}\mathbf{w}_1\\ \mathbf{w}_2\end{bmatrix} = \begin{bmatrix}\hat{\mathbf{S}} & \mathbf{0}\\ \mathbf{0} & \mathbf{I}\end{bmatrix}\begin{bmatrix}\hat{\mathbf{x}}_1\\ \hat{\mathbf{x}}_2\end{bmatrix} = \mathbf{K}\hat{\mathbf{x}}. \tag{12}$$

Combine the two steps to relate $\mathbf{x}$ and $\mathbf{w}$:

$$\mathbf{w} = \mathbf{K}\mathbf{U}^\top \mathbf{x}. \tag{13}$$

In terms of $\mathbf{w}$, (9) becomes

$$\min \quad \mathbf{w}^\top \mathbf{B}\mathbf{w} + \mathbf{w}^\top \mathbf{b} \tag{14a}$$
$$s.t. \quad \mathbf{w}_1^\top \mathbf{w}_1 = c, \tag{14b}$$

where

$$\mathbf{B} = \mathbf{K}^{-1}\mathbf{U}^\top \mathbf{N}_1^\top \mathbf{Q}_{\text{obj}}\mathbf{N}_1 \mathbf{U}\mathbf{K}^{-1}$$
$$\mathbf{b} = 2\mathbf{K}^{-1}\mathbf{U}^\top \mathbf{N}_1^\top \mathbf{Q}_{\text{obj}}\mathbf{z}_1^*.$$

The manipulations in this section have restored the norm structure of the quadratic constraint.

D. Elimination of unconstrained variables

Next we will use the KKT conditions of (14) to eliminate $\mathbf{w}_2$, which consists of unconstrained variables. Begin by expanding the objective:

$$\begin{aligned} f(\mathbf{w}) &= \begin{bmatrix}\mathbf{w}_1^\top & \mathbf{w}_2^\top\end{bmatrix}\begin{bmatrix}\mathbf{B}_{11} & \mathbf{B}_{12}\\ \mathbf{B}_{12}^\top & \mathbf{B}_{22}\end{bmatrix}\begin{bmatrix}\mathbf{w}_1\\ \mathbf{w}_2\end{bmatrix} + \begin{bmatrix}\mathbf{w}_1^\top & \mathbf{w}_2^\top\end{bmatrix}\begin{bmatrix}\mathbf{b}_1\\ \mathbf{b}_2\end{bmatrix} \\ &= \mathbf{w}_1^\top \mathbf{B}_{11}\mathbf{w}_1 + 2\mathbf{w}_1^\top \mathbf{B}_{12}\mathbf{w}_2 + \mathbf{w}_2^\top \mathbf{B}_{22}\mathbf{w}_2 \\ &\quad + \mathbf{w}_1^\top \mathbf{b}_1 + \mathbf{w}_2^\top \mathbf{b}_2. \end{aligned}$$

Next, set the partial derivative with respect to $\mathbf{w}_2$ equal to zero:

$$\begin{aligned} \frac{\partial f}{\partial \mathbf{w}_2} &= 2\mathbf{w}_2^\top \mathbf{B}_{22} + 2\mathbf{w}_1^\top \mathbf{B}_{12} + \mathbf{b}_2^\top = \mathbf{0} \\ \implies \mathbf{w}_2 &= -\mathbf{B}_{22}^{-1}\left(\mathbf{B}_{12}^\top \mathbf{w}_1 + \frac{1}{2}\mathbf{b}_2\right). \end{aligned} \tag{15}$$

After substitution of (15), the objective depends only on $\mathbf{w}_1$:

$$\begin{aligned} f(\mathbf{w}_1) = \mathbf{w}_1^\top &\left(\mathbf{B}_{11} - \mathbf{B}_{12}\mathbf{B}_{22}^{-1}\mathbf{B}_{12}^\top\right)\mathbf{w}_1 \\ &+ \mathbf{w}_1^\top(\mathbf{b}_1 - \mathbf{B}_{12}\mathbf{B}_{22}^{-1}\mathbf{b}_2). \end{aligned}$$

(The constant term, which plays no role in minimization, was omitted.) Thus, (14) is equivalent to a n_t-dimensional program with a single norm constraint:

$$\min \quad \mathbf{w}_1^\top \hat{\mathbf{B}}\mathbf{w}_1 - 2\mathbf{w}_1^\top \hat{\mathbf{b}} \tag{16a}$$
$$s.t. \quad \mathbf{w}_1^\top \mathbf{w}_1 = c, \tag{16b}$$

where

$$\hat{\mathbf{B}} = \mathbf{B}_{11} - \mathbf{B}_{12}\mathbf{B}_{22}^{-1}\mathbf{B}_{12}^\top$$
$$\hat{\mathbf{b}} = -\frac{1}{2}\left(\mathbf{b}_1 - \mathbf{B}_{12}\mathbf{B}_{22}^{-1}\mathbf{b}_2\right).$$

E. Solution via iteration

A straightforward method of solving (16) involves initially diagonalizing $\hat{\mathbf{B}}$ (by the process described in Section IV-C). Now let v be the Lagrange multiplier associated with the constraint (16b), and write the first-order optimality conditions:

$$\hat{\mathbf{B}}\mathbf{w}_1 = v\mathbf{w}_1 \ + \hat{\mathbf{b}} \tag{17a}$$
$$\mathbf{w}_1^\top \mathbf{w}_1 = c \tag{17b}$$

This system is equivalent to the *secular equation*

$$f(v) = \sum_{i=1}^{n}\left(\frac{\hat{\mathbf{b}}_i}{\hat{\mathbf{B}}_{i,i} - v}\right)^2 - c,$$

which has between 2 and $2n_t$ solutions.[4] Obtaining all solutions would require traversing the curve from each pole (nonzero diagonal element of $\hat{\mathbf{B}}$) in both directions. Fortunately, the proof in Appendix B shows that optimizing (16) is equivalent to minimizing v subject to (17). Because $\mathbf{w}_1^\top \mathbf{w}_1$ is a monotonically increasing function of v from $-\infty$ to the smallest nonzero diagonal element of $\hat{\mathbf{B}}$, we can obtain the smallest feasible value of v using the following iterative relationship (due to [18]):

$$v^{(i+1)} = v^{(i)} - 2\frac{f\left(v^{(i)}\right) + c}{f'\left(v^{(i)}\right)}\sqrt{\frac{f\left(v^{(i)}\right) + c}{c}} - 1.$$

[4]This is apparent from the graph of a secular equation. See [18].

The value of v obtained at convergence corresponds to the optimal $\mathbf{w}_1$ in (16). Reversing all variable changes yields the optimal value for $\mathbf{z}$ in the original solution space. This vector specifies wind site active power deviations, voltage angles, and the active power mismatch at each time step.

Each line in the network has its own QCQP and solution vector $\mathbf{z}$. Once each line's QCQP has been solved, the set of solution vectors may be sorted by objective value (6a). Lines whose solutions have small objective value are more likely to reach unacceptable temperatures due to changes in wind; lines with large objective value are comparatively robust to wind fluctuations. The vector $\mathbf{z}$ with lowest objective is the *instanton*.

V. Implementation

We focus on implementation details in two areas: pre-analysis checks to rule out infeasible QCQPs, and numerical considerations that determine overall computational requirements and scaling.

A. Pre-analysis checks

Pre-analysis checks can identify two situations that lead to infeasible temporal instanton QCQPs. First, if a line's resistance is zero, it must be excluded.[5] Equation (21) indicates power loss will be zero for such lines regardless of flow, so wind variations have no effect on their temperature. The second check makes use of injection shift factors. Suppose a network's topology and wind site placement is such that power flow for a particular line is completely unaffected by changes in wind generation. In this scenario, line temperature is isolated from changes in decision variables, and our QCQP is infeasible. Fortunately, DC injection shift factors may be used to skip such lines: whenever a line's flow is detached from changes in wind, its shift factors with respect to all wind nodes will be zero.

B. Computational burden and algorithm scaling

Temporal instanton analysis consists of solving a Section III QCQP via the Section IV method for each line in the network. Each QCQP is independent from, and nearly identical to, all others.[6] This pleasing parallelism means total processing time grows linearly with the number of lines analyzed. In the remainder of this section we focus on individual QCQPs. Solution time for a single QCQP varies with network size, wind site placement, and algorithm design. Reasoning from algorithmic complexity and numerical results, we call attention to considerations that characterize scaling.

Sparsity is of the utmost importance in numerical implementation of temporal instanton analysis. Because each piece of (6) is dominated by zeros, sparsity plays a key role in storage requirements before manipulations even begin. The objective, for example, contains only a subset $\mathbf{z}_1$ of the variables; portions of $\mathbf{Q}_{\text{obj}}$ corresponding to $\mathbf{z}_2$ and $\mathbf{z}_3$ consist entirely of zeros. Even the nonzero portion of $\mathbf{Q}_{\text{obj}}$ (the precision matrix $\mathbf{Q}$) is sparse if the method of [14] is used to generate it. The constraints (6b) and (6c) are similarly sparse: a dense representation of (6b) for the RTS-96 network with six time steps occupies 2.5 megabytes; a sparse version takes just 40 bytes. The benefits of sparsity carry through to concatenation, multiplication, and factorization.

Matrix factorization, a relatively expensive operation, plays a significant role in determining overall algorithm scaling. Three factorizations are required in the Section IV solution method. First, a portion of the $\mathbf{A}$ matrix must be factorized to find its pseudoinverse and determine the min-norm translation point $\mathbf{z}^*$ in (7). A sparse Cholesky factorization is appropriate here. A second factorization is necessary to construct a basis for the kernel of $\mathbf{A}$. Here one might use a sparse QR factorization or, if the $\mathbf{A}$ matrix is well-conditioned, an LU-based approach to save time.[7] Another necessary factorization is the singular value decomposition required for diagonalizing the constraint (see Section IV-C). Because $\mathbf{N}_3$ is $n_r n_t$-by-n_t, it has only n_t nonzero singular values. These may be found directly using a dense SVD algorithm, but it is more efficient to retrive them via Arnoldi iteration.[8] The fourth factorization is less demanding: block LU decomposition may be used to inexpensively expose the Schur complements needed to compute $\hat{\mathbf{B}}$ and $\hat{\mathbf{b}}$ in (16); see [21].

We performed two tests to characterize scaling of our algorithm. First, we varied the number of wind nodes (and, therefore, decision variables) in the RTS-96 network and, considering a time horizon of one hour divided into six ten-minute intervals, performed a complete analysis in each case. Figure 2 illustrates the relationship between QCQP size and the average QCQP solution time. Second, we added wind farms to ten of the test cases packaged with MATPOWER [22] and analyzed each. For each network we replaced a fixed portion of conventional generation with wind, placed wind sites randomly, and sized each site to fix overall wind penetration to 70%. The choice of these parameters is somewhat arbitrary for the purposes of characterizing algorithm scaling, but we were careful to add enough significantly-sized wind farms to each network to avoid numerical difficulties.[9] Figure 3 shows average computation time for a single QCQP versus network size. As a reference point for overall solution time, it took just over two hours for our four-core laptop with 8 GB of RAM to analyze every line in the Polish summer 2008 peak network (case `3120sp` in Matpower). The same analysis applied to the RTS-96 network takes roughly half a second.

VI. Results

Numerical results are included for two purposes. The first is to illustrate the relationship between the instanton pattern

[5] Of course, zero-resistance lines are more an artifact of network bookkeeping than a physical reality.

[6] Only the n_t rows of $\mathbf{A}$ corresponding to auxiliary angle variables $\hat{\theta}$ change as one line is replaced by another.

[7] The SPQR algorithm in SuiteSparse [19] is well suited for the QR-based approach. The LU approach involves column operations on the $\mathbf{A}$ matrix augmented with identity below. If QR factorization is used, this step takes more than a third of total computation time.

[8] An appropriate algorithm is described in [20] and implemented in ARPACK. It is available in MATLAB, SciPy, and Julia environments through the `eigs` and `svds` functions.

[9] If there are too few wind nodes or penetration is too low, many solutions will have absurdly high objective value.

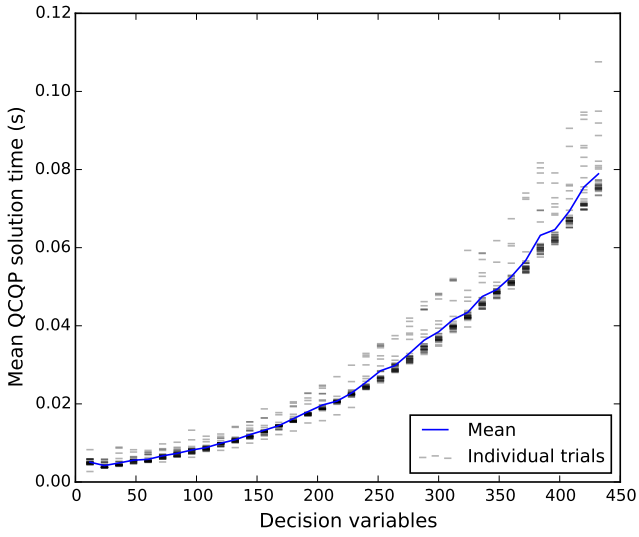

Fig. 2. Average computation time per QCQP solution versus number of decision variables. The network is the 73-node RTS-96, and the time horizon is one hour divided into six ten-minute intervals. Starting with two, the number of wind farms is increased two at a time up to 72, and these wind farms are randomly placed throughout the network. The ratio of forecast wind generation to conventional generation is fixed at 0.7. Analysis was repeated thirty times to illustrate the effects of wind farm placement on solution times; light gray lines indicate average QCQP solution times for individual trials.

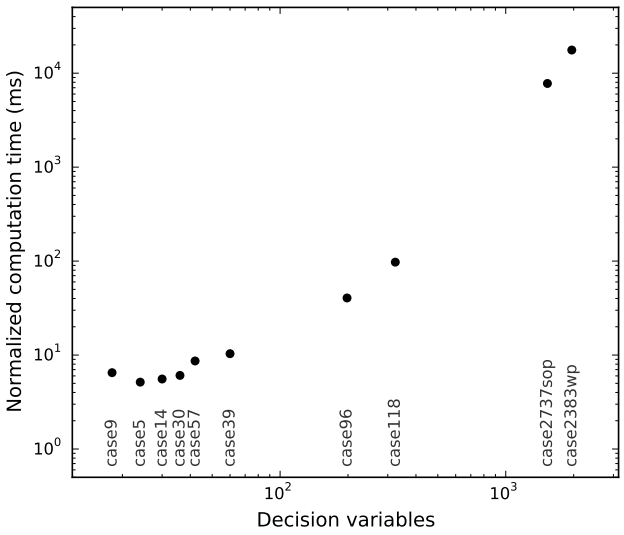

Fig. 3. Average computation time (total time divided by number of lines analyzed) for ten Matpower cases, on a log-log scale. For each network, the number of wind farms is equal to the number of conventional generators, and wind nodes were chosen randomly. In every case the time horizon is five minutes divided into six thirty-second intervals.

and a line's temperature trajectory. How does line temperature evolve in response to instanton angle differences? Second, numerical experimentation can illustrate the effects of wind covariance. What impact does a reasonable covariance matrix have on instanton objective values and wind patterns? In each experiment we used the modified RTS-96 network from [23], assumed Waxwing conductors as in [24], considered six time steps, and gradually increased the wind forecast over time while keeping conventional generation and demand constant.

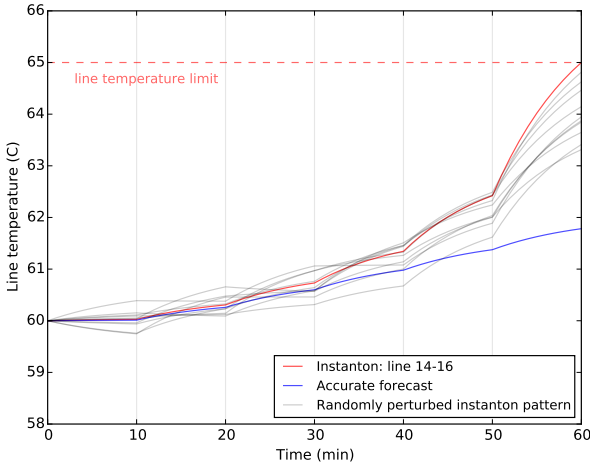

Fig. 4. RTS-96 temperature trajectories for the line between nodes 14 and 16. Red represents the instanton trajectory, which brings the line to its temperature limit of 65 C. Trajectories shown in gray arise from randomly perturbed versions of the instanton wind pattern having the same objective value. The blue trajectory corresponds to zero deviation from the wind forecast.

A. *Temperature Trajectories*

We assume all lines begin at $60°$C and have temperature limits of $65°$C. We performed instanton analysis for a one-hour time horizon divided into six ten-minute intervals. Figure 4 illustrates temperature trajectories corresponding to the instanton and nearby wind patterns. The instanton pattern causes the line to reach $65°$C, but if we randomly perturb the vector of forecast deviations while keeping its norm (objective value) constant, the line does not reach its temperature limit. This illustrates that the solution found by our algorithm is the most likely wind forecast deviation pattern with respect to the wind model described in Section II-B.

B. *Effects of Covariance*

To illustrate the effects of covariance on temporal instanton analysis, we used a simple heuristic method to generate a reasonable spatial covariance matrix for the RTS-96. After assigning geographic coordinates to each of the eighteen wind farms and constructing a distance matrix, we mapped distances to correlation coefficients using a relationship from [15]. This positive-definite, unit-norm covariance matrix weights wind deviations at all time steps, allowing the QCQP solution algorithm to find patterns with lower objective value by increasing highly correlated deviations. Figure 5 shows that these patterns have higher objective value when the original objective function (simple two-norm) is used.

VII. Conclusion

This paper has extended the temporal instanton analysis method presented in [10] with a focus on implementation and algorithm scaling. Models for each of the three phenomena involved in temporal instanton analysis were presented and combined into a QCQP, and a solution algorithm was presented. Important numerical considerations were then discussed, and algorithm scaling was illustrated. Finally, numerical results were presented to show temperature trajectories and the effects of wind covariance.

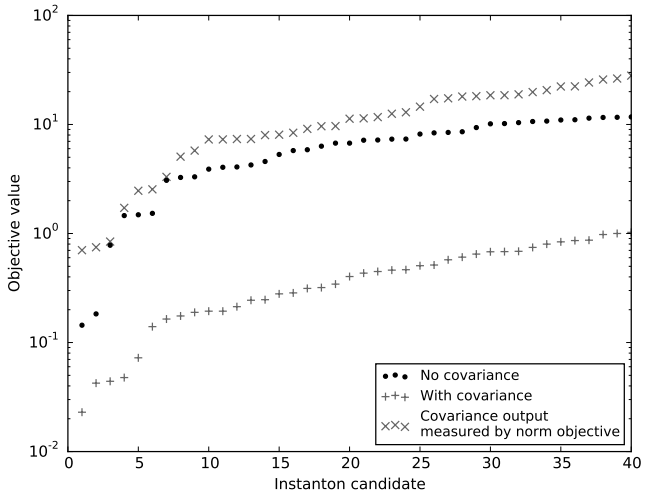

Fig. 5. Objective values for lowest forty instanton candidates, with and without covariance. "Covariance output measured by norm objective" was computed by passing solution vectors from the covariance analysis output to the objective function from the no-covariance case.

APPENDIX A
LINE TEMPERATURE MODEL

The change in temperature of any object may be expressed as a differential equation called the heat balance equation, which relates temperature change to a sum of various sources of heating. The IEEE 738 standard [11] provides the following heat balance equation for a transmission line:

$$\frac{dT}{dt} = \frac{1}{m \cdot C_p}\left[I^2 \cdot R(T_{\mathrm{l,C}}(t)) - q_c - q_r + q_s\right] \tag{18}$$

In (18), $T_{\mathrm{l,C}}(t)$ is the conductor average temperature in Celsius, $m \cdot C_p$ is the product of mass and heat capacity, and $I^2 \cdot R(T_{\mathrm{l,C}}(t))$ represents heat rate due to resistive heating. q_c represents convective heat loss, which is proportional to the temperature difference between the line and surrounding air:

$$q_c = \eta_c \cdot (T_{\mathrm{l,C}}(t) - T_{\mathrm{a,C}}) \ , \tag{19}$$

where $T_{\mathrm{a,C}}$ is the ambient temperature in Celsius. q_r in (18) represents radiation heat loss, modeled by the fourth-order expression

$$q_r = \eta_r \cdot \left[T_{\mathrm{l,K}}(t)^4 - T_{\mathrm{a,K}}^4\right] , \tag{20}$$

where $T_{\mathrm{l,K}}(t)$ and $T_{\mathrm{a,K}}$ are the conductor and ambient temperatures in Kelvin, respectively. Finally, q_s in (18) represents solar heating. In this paper q_s is fixed to some conservative constant (corresponding to full, direct sun).

We replace the resistive heat rate term $I^2 \cdot R(T_{\mathrm{l,C}}(t))$ by f_{ij}^{loss}, the approximate line loss expression derived in [12]:

$$f_{ij}^{\mathrm{loss}} \approx r_{ij}\left(\frac{\theta_{ij}}{x_{ij}}\right)^2 , \tag{21}$$

where θ_{ij} is the difference between angles θ_i and θ_k, and $r_{ij} + jx_{ij}$ is the impedance of the line between nodes i and j. Three DC power flow assumptions underpin (21): voltage magnitudes are all 1pu, cosine may be approximated by its second-order Taylor expansion, and $x_{ij} \geq 4r_{ij}$. Thus, (21) provides an approximates line losses using voltage angle differences.

When (18) is combined with an initial temperature $T_{\mathrm{l,C}}^0$ and (21), the resulting initial value problem should make it possible to determine conductor temperature $T_{\mathrm{l,C}}(t_n)$ at a later time t_n. We substitute (19)-(21) into (18) and attempt to solve for temperature:

$$\frac{dT}{dt} = \frac{1}{mC_p}\big[f_{ij}^{\mathrm{loss}} - \eta_c\left(T_{\mathrm{l,C}}(t) - T_{\mathrm{a,C}}\right) - \eta_r\left(T_{\mathrm{l,K}}(t)^4 - T_{\mathrm{a,K}}^4\right) + q_s\big] \tag{22}$$

If power flow, ambient temperature, and solar heat rate are constant, this differential equation is still fourth-order in conductor temperature $T_{\mathrm{C}}(t)$ due to radiation. Fortunately, q_r is approximately linear over our temperature range of interest (from ambient temperature to temperature limit). We replace q_r by the conservative linearization[10]

$$\tilde{q}_r = \eta_r\left(T_{\mathrm{m,K}}^4 - T_{\mathrm{a,K}}^4\right) + 4\eta_r T_{\mathrm{m,K}}^3(T_{\mathrm{l,C}}(t) - T_{\mathrm{m,C}}), \tag{23}$$

where $T_{\mathrm{m,C}}$ is the average (midpoint between) ambient and conductor limit temperatures in Celsius, and $T_{\mathrm{m,K}}$ is $T_{\mathrm{m,C}}$ converted to Kelvin. After substitution of (23), the heat balance equation becomes linear in conductor temperature, and the IVP has a straightforward solution.

Substitution of (23) into (22) yields the approximate heat balance equation

$$\frac{dT_{\mathrm{l,C}}}{dt} = aT_{\mathrm{l,C}}(t) + b \ , \tag{24}$$

where constants a and b are defined as

$$a = \frac{1}{mC_p}\left[-\eta_c - 4\eta_r T_{\mathrm{m,K}}^3\right] \tag{25a}$$

$$b = \frac{1}{mC_p}\big[f_{ij}^{\mathrm{loss}} + \eta_c T_{\mathrm{a,C}} - \eta_r\left(T_{\mathrm{m,K}}^4 - T_{\mathrm{a,K}}^4\right) + 4\eta_r T_{\mathrm{m,C}} \cdot T_{\mathrm{m,K}}^3 + q_s\big] \tag{25b}$$

The IVP (24) has a straightforward solution:

$$T_{\mathrm{l,C}}(t) = ke^{at} - \frac{b}{a}, \tag{26}$$

where $k = T_{\mathrm{l,C}}(0) + b/a$. Note that b is influenced by power flow (via f_{ij}^{loss} according to (21)), but a is not. The only variables in (26) are initial temperature and angle differences during each time interval. There is therefore a recursive relationship between final temperature and initial temperature that involves only angle differences. The derivation of this recursive relationship is an exercise in messy linear algebra; it is omitted here for brevity. The final relationship is expressed in (1), where it is used as a line temperature constraint.

[10]Because a transmission line is hotter than surrounding air, radiation tends to decrease line temperature. Thus, a conservative approach will underestimate q_r. Plotting (23) shows that it does indeed underestimate q_r.

APPENDIX B
LAGRANGE MULTIPLIER PROOF

A. Statement

The following two optimization problems are equivalent:

$$\begin{aligned} (P) \quad & \min \ \mathbf{w}^\top \hat{\mathbf{B}} \mathbf{w} - 2\hat{\mathbf{b}}^\top \mathbf{w} \\ s.t. \quad & \mathbf{w}^\top \mathbf{w} = c \\ (P') \quad & \min \ u \\ s.t. \quad & \mathbf{w}^\top \mathbf{w} = c \qquad (27a) \\ & \hat{\mathbf{B}} \mathbf{w} = u\mathbf{w} + \hat{\mathbf{b}} \ . \qquad (27b) \end{aligned}$$

(Note that $\hat{\mathbf{B}}$ is diagonal, and (P) is equivalent to (16).)

B. Proof

It is sufficient to prove that if $(u_1, \mathbf{w}_1)$ and $(u_2, \mathbf{w}_2)$ satisfy the first-order conditions (27a)-(27b) with $u_1 < u_2$, then

$$f(\mathbf{w}_1) = \mathbf{w}_1^\top \hat{\mathbf{B}} \mathbf{w}_1 - 2\hat{\mathbf{b}}^\top \mathbf{w}_1 < \mathbf{w}_2^\top \hat{\mathbf{B}} \mathbf{w}_2 - 2\hat{\mathbf{b}}^\top \mathbf{w}_2 = f(\mathbf{w}_2).$$

We proceed using a technique from [18]. By (27a) we have:

$$\hat{\mathbf{B}} \mathbf{w}_1 = u_1 \mathbf{w}_1 + \hat{\mathbf{b}} \qquad (28a)$$

$$\hat{\mathbf{B}} \mathbf{w}_2 = u_2 \mathbf{w}_2 + \hat{\mathbf{b}} \qquad (28b)$$

Multiply both (28a) and (28b) by $\mathbf{w}_1^\top$ and $\mathbf{w}_2^\top$ to obtain

$$\mathbf{w}_1^\top \hat{\mathbf{B}} \mathbf{w}_1 = u_1 c + \mathbf{w}_1^\top \hat{\mathbf{b}} \qquad (29a)$$

$$\mathbf{w}_2^\top \hat{\mathbf{B}} \mathbf{w}_2 = u_2 c + \mathbf{w}_2^\top \hat{\mathbf{b}} \qquad (29b)$$

$$\mathbf{w}_1^\top \hat{\mathbf{B}} \mathbf{w}_2 = u_2 \mathbf{w}_1^\top \mathbf{w}_2 + \hat{\mathbf{b}}^\top \mathbf{w}_1 \qquad (29c)$$

$$\mathbf{w}_2^\top \hat{\mathbf{B}} \mathbf{w}_1 = u_1 \mathbf{w}_2^\top \mathbf{w}_1 + \hat{\mathbf{b}}^\top \mathbf{w}_2, \qquad (29d)$$

where (27b) was used to replace instances of $\mathbf{w}_1^\top \mathbf{w}_1$ and $\mathbf{w}_2^\top \mathbf{w}_2$ with c. Now subtract (29b) from (29a) to obtain

$$(\mathbf{w}_1^\top \hat{\mathbf{B}} \mathbf{w}_1 - \mathbf{w}_1^\top \hat{\mathbf{b}}) - (\mathbf{w}_2^\top \hat{\mathbf{B}} \mathbf{w}_2 - \mathbf{w}_2^\top \hat{\mathbf{b}}) = (u_1 - u_2)c.$$

Add $\hat{\mathbf{b}}^\top \mathbf{w}_2$ and subtract $\hat{\mathbf{b}}^\top \mathbf{w}_1$ to yield

$$f(\mathbf{w}_1) - f(\mathbf{w}_2) = (u_1 - u_2)c - \mathbf{w}_1^\top \hat{\mathbf{b}} + \mathbf{w}_2^\top \hat{\mathbf{b}},$$

then substitute (29c) and (29d):

$$\begin{aligned} f(\mathbf{w}_1) - f(\mathbf{w}_2) &= (u_1 - u_2)c + (u_2 - u_1)\mathbf{w}_1^\top \mathbf{w}_2 \\ &= (u_1 - u_2)(c - \mathbf{w}_1^\top \mathbf{w}_2) \end{aligned}$$

Note that $\|\mathbf{w}_1 - \mathbf{w}_2\| = \mathbf{w}_1^\top \mathbf{w}_1 + \mathbf{w}_2^\top \mathbf{w}_2 - 2\mathbf{w}_1^\top \mathbf{w}_2 = 2c - 2\mathbf{w}_1^\top \mathbf{w}_2$, so

$$f(\mathbf{w}_1) - f(\mathbf{w}_2) = \frac{1}{2}(u_1 - u_2)\|\mathbf{w}_1 - \mathbf{w}_2\|.$$

Because $u_1 < u_2$, the right-hand size is negative. The objective value corresponding to $\mathbf{w}_1$ is therefore less than that of $\mathbf{w}_2$. We conclude that (P) and (P') are equivalent.

REFERENCES

[1] J. Rogers, S. Fink, and K. Porter, "Examples of wind energy curtailment practices," 2010.

[2] B. Parsons, M. Milligan, B. Zavadil, D. Brooks, B. Kirby, K. Dragoon, and J. Caldwell, "Grid impacts of wind power: a summary of recent studies in the united states," *Wind Energy*, vol. 7, no. 2, pp. 87–108, 2004.

[3] M. Chertkov, F. Pan, and M. Stepanov, "Predicting failures in power grids: The case of static overloads," *IEEE Transactions on Smart Grid*, vol. 2, no. 1, pp. 162–172, Mar. 2011.

[4] M. Chertkov, M. Stepanov, F. Pan, and R. Baldick, "Exact and efficient algorithm to discover extreme stochastic events in wind generation over transmission power grids," in *Proc. 2011 50th IEEE Conference on Decision and Control and European Control Conference (CDC-ECC)*, 2011, pp. 2174–2180.

[5] S. Baghsorkhi and I. Hiskens, "Analysis tools for assessing the impact of wind power on weak grids," in *Proc. Systems Conference (SysCon), 2012 IEEE International*, 2012, pp. 1–8.

[6] C. Coffrin, P. Van Hentenryck, and R. Bent, "Approximating line losses and apparent power in AC power flow linearizations," pp. 1–8.

[7] H. Hijazi, C. Coffrin, and P. Van Hentenryck, "Convex quadratic relaxations of nonlinear programs in power systems," *Optimization Online*, 2013. [Online]. Available: http://www.optimization-online.org/DB_FILE/2013/09/4057.pdf

[8] C. Coffrin and P. Van Hentenryck, "A Linear-Programming Approximation of AC Power Flows," *INFORMS Journal on Computing*, vol. 26, no. 4, pp. 718–734, Nov. 2014. [Online]. Available: http://pubsonline.informs.org/doi/abs/10.1287/ijoc.2014.0594

[9] H. Banakar, N. Alguacil, and F. Galiana, "Electrothermal coordination part I: theory and implementation schemes," *IEEE Transactions on Power Systems*, vol. 20, no. 2, pp. 798–805, May 2005.

[10] J. Kersulis, I. Hiskens, M. Chertkov, S. Backhaus, and D. Bienstock, "Temperature-based instanton analysis: Identifying vulnerability in transmission networks," in *PowerTech, 2015 IEEE Eindhoven*, Jun. 2015, pp. 1–6.

[11] "IEEE Standard for Calculating the Current-Temperature Relationship of Bare Overhead Conductors," *IEEE Std 738-2012 (Revision of IEEE Std 738-2006 - Incorporates IEEE Std 738-2012 Cor 1-2013)*, pp. 1–72, Dec. 2013.

[12] M. Almassalkhi and I. Hiskens, "Model-predictive cascade mitigation in electric power systems with storage and renewables – part I: Theory and implementation," *IEEE Transactions on Power Systems*, vol. PP, no. 99, pp. 1–11, 2014.

[13] B. Hodge and M. Milligan, "Wind power forecasting error distributions over multiple timescales," in *2011 IEEE Power and Energy Society General Meeting*, Jul. 2011, pp. 1–8.

[14] J. Tastu, P. Pinson, and H. Madsen, "Space-time trajectories of wind power generation: Parameterized precision matrices under a Gaussian copula approach," in *Modeling and Stochastic Learning for Forecasting in High Dimensions*, ser. Lecture Notes in Statistics, X. Brossat, Ed. Springer, 2015, pp. 267–296.

[15] L. Freris and D. Infield, *Renewable energy in power systems*. John Wiley & Sons, 2008.

[16] D. Bienstock and A. Michalka, "Polynomial Solvability of Variants of the Trust-region Subproblem," in *Proceedings of the Twenty-Fifth Annual ACM-SIAM Symposium on Discrete Algorithms*, ser. SODA '14. Portland, Oregon: SIAM, 2014, pp. 380–390. [Online]. Available: http://dl.acm.org/citation.cfm?id=2634074.2634102

[17] O. Mehanna, K. Huang, B. Gopalakrishnan, A. Konar, and N. Sidiropoulos, "Feasible point pursuit and successive approximation of non-convex QCQPs," *IEEE Signal Processing Letters*, vol. PP, no. 99, pp. 1–1, 2014.

[18] W. Gander, G. H. Golub, and U. von Matt, "A constrained eigenvalue problem," vol. 114-115, pp. 815–839. [Online]. Available: http://www.sciencedirect.com/science/article/pii/0024379589904941

[19] L. V. Foster and T. Davis, "Reliable calculation of numerical rank, null space bases, basic solutions and pseudoinverse solutions using suitesparseqr," in *Householder Symposium XVIII on Numerical Linear Algebra*, 2011, p. 79.

[20] R. B. Lehoucq and D. C. Sorensen, "Deflation techniques for an implicitly restarted arnoldi iteration," *SIAM Journal on Matrix Analysis and Applications*, vol. 17, no. 4, pp. 789–821, 1996.

[21] F. Zhang, *The Schur complement and its applications*. Springer Science & Business Media, 2006, vol. 4.

[22] R. D. Zimmerman, C. E. Murillo-Sánchez, and R. J. Thomas, "Matpower: Steady-state operations, planning, and analysis tools for power systems research and education," *Power Systems, IEEE Transactions on*, vol. 26, no. 1, pp. 12–19, 2011.

[23] H. Pandzic, Y. Dvorkin, T. Qiu, Y. Wang, and D. Kirschen. Unit Commitment under Uncertainty - GAMS Models, Library of the Renewable Energy Analysis Lab (REAL), University of Washington, Seattle, USA.

[24] M. Almassalkhi and I. Hiskens, "Model-predictive cascade mitigation in electric power systems with storage and renewables – part II: Case-study," vol. 30, no. 1, pp. 78–87.